An Online Conference
NOISE-CON 2020
Week of November 16, 2020

# Evaluation of embedded windshield resonators to reduce cabin noise of a UAM concept aircraft

Matthew B. Galles
Albert R. Allen
Structural Acoustics Branch
NASA Langley Research Center
Mail Stop 463
Hampton, VA 23681
matthew.b.galles@nasa.gov

## ABSTRACT

High cabin noise levels in UAM vehicles could affect passenger comfort and thus passenger acceptance of this class of aircraft. As windshields will likely comprise a large percentage of the surface area of a UAM aircraft fuselage, the objective of this work was to explore the feasibility of a noise reduction concept that utilizes the windshield area. The concept aims to increase interior absorption at targeted frequencies by assuming that a honeycomb-like array of interior facing acoustic resonators are embedded within multiple transparent layers that make up the front and side windshields. The vehicle considered was based on the NASA RVLT Lift+Cruise UAM concept, which has 7.2 $m^2$ of front- and side-facing windshields. Statistical Energy Analysis was used to evaluate the noise reduction attributed to the inclusion of various resonator configurations. The predicted noise reduction was dependent on the resonator geometry, the quantity of resonators included, and the assumed baseline interior cabin absorption. Results from a variety of resonator configurations are shown and discussed. The optical feasibility of the concept is not discussed in this work.

## 1 INTRODUCTION

A large percentage of the fuselage of many vehicles developed for the Urban Air Mobility (UAM) market is comprised of front- and side-facing windshields. While there are many noise treatment options available for aircraft fuselages, few options are available to treat cabin noise that exploit the large windshield surface area. As a result, a noise treatment was studied that could be embedded within the windshields to increase the noise reduction in the vehicle cabin.

The rotors used to provide lift for UAM concept vehicles like the NASA RVLT Lift+Cruise reference aircraft are expected to produce tonal noise in frequency bands near the blade pass frequency (BPF) of 40 Hz.[1] A low profile hexagonal array of cavities allows for resonator cavity volumes to be sized to absorb noise in frequency bands relevant to these vehicles. The embedded windshield resonators reduce cabin noise by increasing the absorption area of the windshield, thereby providing a noise treatment that takes advantage of the windshield's large surface area. Another unique benefit of this concept is that it can provide sound absorption without a substantial increase in structure mass or windshield thickness – which ranges from 0.1″ to 0.375″ in helicopters and general aviation aircraft. The optical viability of such a concept is not considered

here, but rather the goal of this paper is to motivate further research to develop this concept as a viable noise treatment.

Resonators have been used with the intention to improve acoustics since antiquity; an interesting example is in the design of the ancient theater of Lyttus in Crete, which contained 13 "acoustic vases" that were Helmholtz resonators.[2,3] From the middle ages and early modern period, over 50 churches have been identified that contain vases, or resonators, the purpose of which is most probably acoustic.[3] More recently, Kuntz et al.[4] investigated the benefits of embedding acoustic resonators in the sidewalls of an aircraft cabin to increase the sidewall transmission loss at the propfan BPFs. Lane et al.[5] investigated a method to damp low-frequency resonant noise using resonators, called chamber cores, which were incorporated into the sandwich structure of the fairing walls of a launch vehicle. Allen et al.[6] investigated adding foam treatments to structurally integrated resonators in a corrugated-core sandwich structure representative of an aircraft fuselage and found that inclusion of fuselage integrated resonators can supplement interior noise control at lower frequencies, but will have little additional effect if the preexisting interior treatment is adequate. The literature shows that resonators can be effective in damping noise at certain frequencies, which is important for applications consisting of largely tonal noise, such as the noise generated at harmonics of a propeller's BPF.

In this paper, a resonator concept suitable for incorporation into a thin windshield will be presented, including a physical description and the mechanism that provides additional noise reduction in the cabin interior. Then, the Statistical Energy Analysis (SEA) tool that was created to estimate the benefits of this concept will be presented using a model of the NASA RVLT Lift+Cruise reference vehicle.[1] Finally, the additional noise reduction due to the inclusion of embedded resonators will be discussed.

## 2 CONCEPT

Aircraft windshields are commonly fabricated with a layering process forming laminate plies of polymethyl methacrylate (PMMA) or other materials to satisfy design requirements related to visibility, impact resistance, structural integrity, and other criteria. This laminated design allows for inclusion of air cavities of desired geometry that can be used as resonant absorbers. Creating a honeycomb-like pattern between the laminate plies allows for an efficient arrangement of the resonators. While the proposed concept is hexagonal in nature, the available geometrical variations are numerous and allow for tailoring of the geometry to address the absorption performance of the coupled acoustic space within specific frequency ranges and windshield locations. Embedding cavities in the windshield will introduce optical scattering effects, and thus it is vital to consider visibility requirements when designing the resonator arrangement and geometry. The focus of this study is to assess the potential benefit of the concept in terms of noise reduction within certain frequency bands relevant to the small flying vehicle considered. The impact of the concept on pilot visibility will require additional assessments if its viability for noise control warrants such investigations.

The resonator consists of a hexagonal cavity with an inlet hole that faces the cabin interior, as shown in Fig. 1. Two resonator concepts were designed, herein referred to as type 1 and type 2 resonators. The geometric parameters of both types are presented in Table 1 and the corresponding dimensions are presented in Fig. 2. The resonator geometries differ only in the cavity hexagonal radius; type 1 resonators have a hexagonal radius of 40 mm whereas type 2 resonators have a hexagonal radius of 60 mm. The larger cavity of the type 2 resonator provides a larger reactance at lower frequencies, as will be shown later. The total thickness of both resonator types is 15 mm with a cavity depth of 7 mm. The inner and outer windshield layer thicknesses for this study are 3

***Table 1:*** *Geometric parameters of type 1 and type 2 resonators.*

| Parameter | Type 1 (mm) | Type 2 (mm) |
|---|---|---|
| Interior plate hole radius | 3 | 3 |
| Inner windshield thickness | 3 | 3 |
| Outer windshield thickness | 5 | 5 |
| Vertical wall thickness | 5 | 5 |
| Cavity Thickness | 7 | 7 |
| Cavity hexagonal radius | 40 | 60 |
| Total thickness | 15 | 15 |

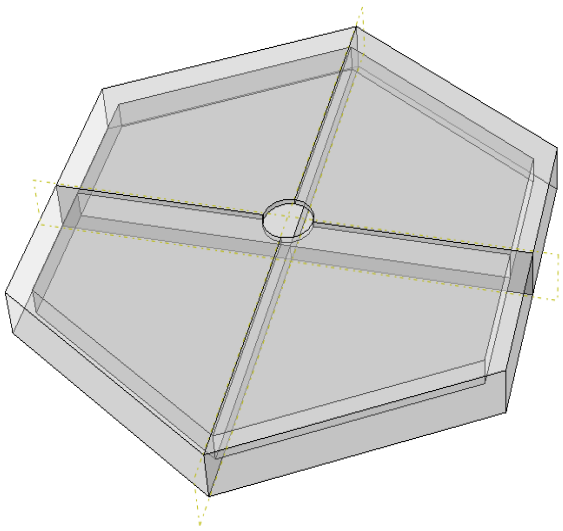

***Figure 1:*** *CAD model of an embedded resonator.*

and 5 mm, respectively. While the proposed windshield is thicker than a typical helicopter windshield, the concept can be designed to have an equivalent area density due to the cavities.

To analyze the benefits of the proposed treatment, it is necessary to estimate the absorption area of the resonator array. The normal incidence absorption area, $A_a$, of each resonator is calculated using the following relationship:[7]

$$A_a = 4\rho_0 c_0 A \frac{\mathrm{Re}(z_{in})}{(z_{in}+z_{rad})^2}, \tag{1}$$

in which $\rho_0$ is the air density, $c_0$ is the air sound speed, $A$ is the resonator inlet area, $z_{in}$ is the specific input impedance of the resonator, and $z_{rad}$ is the specific radiation impedance due to the inlet-coupled half space. The specific radiation impedance is calculated using the baffled piston representation as[8]

$$z_{rad} = \rho_0 c_0 (R + k\chi), \tag{2}$$

in which the radiation resistance is

$$R = \frac{(2ka)^2}{4\cdot 2} - \frac{(2ka)^4}{6\cdot 4^2\cdot 2} - \ldots, \tag{3}$$

in which $k$ is acoustic wavenumber and $a$ is the resonator inlet radius. The radiation reactance is

$$\chi = \frac{4}{\pi}\frac{(2ka)}{3} - \frac{4}{\pi}\frac{(2ka)^3}{5\cdot 3^2} - \ldots, \tag{4}$$

with all higher-order terms not shown in Eqs. (3) and (4) ignored. Calculation of the resonator input impedance is provided below.

The resonator geometries are similar to Helmholtz cavities (see Fig. 3a) and an electrical impedance analogy can be made by modeling an acoustic compliance in series with an acoustic mass representing the thin slug of air near the neck (see Fig. 3b). The input impedance for this lumped element case could be modeled as[9]

$$z_{in} = A\left[ j\omega M_A - \frac{j}{\omega C_A} \right], \tag{5}$$

in which $\omega$ is the angular frequency, $M_A = \rho_0 l/A$ is the acoustic mass, with $l$ being the inlet length, and $C_A = V/\rho_0 c_0^2$ is the acoustic capacitance, with $V$ being the resonator volume. This electrical analogy is shown in Fig. 3, along with the acoustic pressure, $U$. Often, the input impedance of a

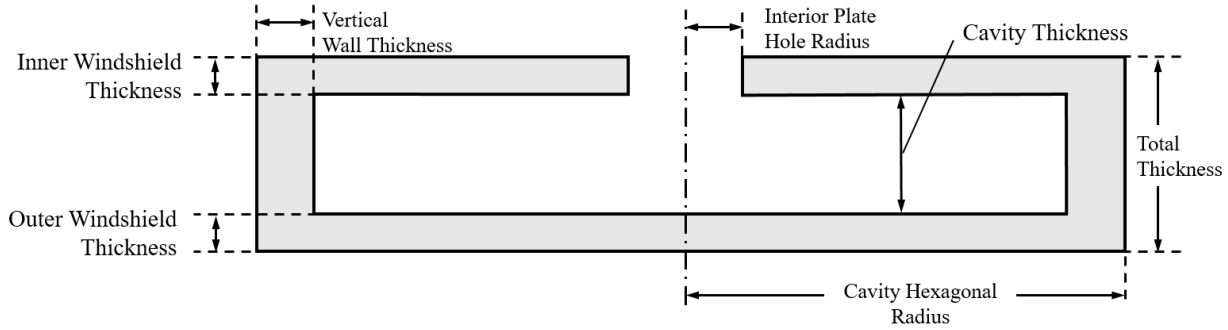


***Figure 2:*** *Geometrical parameters of the resonator concept.*

resonator is modeled using this lumped element approach. However, when the hexagonal radius of the resonator increases, internal cavity modes influence the compliance of the resonator and the lumped element approximation given above no longer holds.

Because of the effects mentioned above, the resonator input impedance is modeled using a commercial finite element (FE) solver[10] instead of the closed-form approximation in Eq. (5). In the FE model, the resonator inlet is connected to a normal incidence tube (NIT) of equivalent diameter, which simulates a typical impedance tube experimental setup used to determine the unknown impedance at the tube termination. The results of the FE model provided the acoustic impedance at the top of the NIT and the terminating impedance of the NIT was calculated as[11]

$$Z_{a,t} = \frac{j(\rho_0 c_0 / A)\sin(kL) - Z_{a,i}\cos(kL)}{j(A/(\rho_0 c_0)Z_{a,i}\sin(kL) - \cos(kL)}, \tag{6}$$

in which $Z_{a,i}$ is the acoustic impedance at the NIT inlet, $k$ is the acoustic wavenumber, and $L$ is the length of the NIT. Because the terminating impedance of the NIT, $Z_{a,t}$, is the input impedance of the resonator at the inlet, the specific input impedance of the resonator, $z_{in}$, can be calculated as

$$z_{in} = Z_{a,t} A. \tag{7}$$

The FE model provides a linear harmonic solution to the Helmholtz equation; that is, the model accounts for the multimodal contributions of the air volume and the mass effects of the air in the resonator neck. Damping was not included in the model, but was subsequently included as an additional frequency independent acoustic resistance of 5 MKS rayls based on experimental data obtained from resonant absorbers with similar inlet geometries.[6] Figure 4 shows the calculated reactances of the type 1 resonator in blue and the type 2 resonator in orange. Note that the type 1 resonator has zero reactance at ~830 Hz and thus provides the most acoustic absorption at this frequency. The type 2 resonator has a near zero reactance from ~400 to ~700 Hz and provides a more broadband acoustic absorption than the type 1 resonator, as will be shown later.

The aircraft windshields are embedded with a number of resonators, $N_r$, which is determined using a ratio of the windshield surface area, $S_{ws}$, to the surface area covered by a resonator, $S_{res}$:

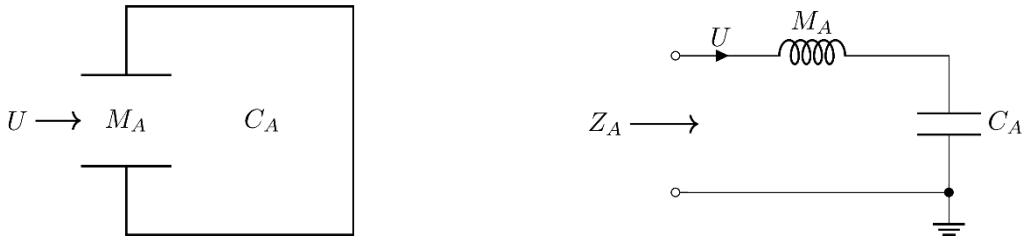


*(a)* *(b)*

***Figure 3:*** *Electrical impedance analogy for a resonator.*

$$N_r = 0.9\frac{S_{ws}}{S_{res}}. \quad (8)$$

The surface area ratio is multiplied by 90% to account for pattern truncations near the edges of the windshield. The absorption areas of the included resonators are summed with the cabin interior absorption area and converted to a damping loss factor, which will be used in the SEA framework presented in Section 3.

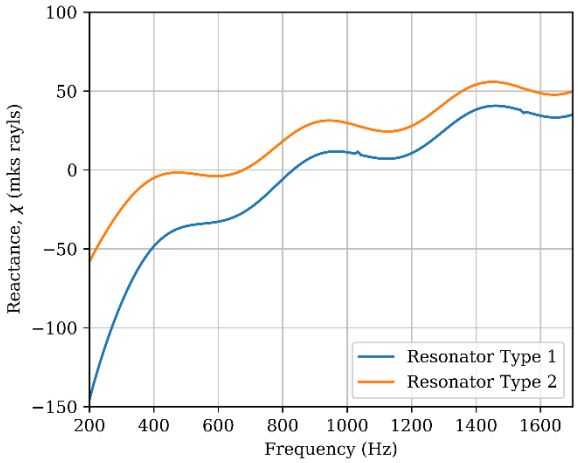


***Figure 4:*** *Reactance of type 1 and type 2 resonators.*

## 3 SIMULATION & RESULTS

In this section, the assumptions used while developing the SEA model will be described, and then the noise reduction attributed to the addition of varied assortments of acoustic resonators will be presented.

### 3.1 Simulation Model

SEA was used to analyze the benefits of the proposed concept using an SEA model that was based on the NASA RVLT Lift+Cruise reference aircraft,[1] shown in Fig. 5. The aircraft fuselage and windshields were modeled as a series of flat plates joined along their perimeters that, when assembled in this manner, enclosed an interior acoustic volume representative of the cabin. The arrangement of the subsystems is shown in Figs. 6 & 7. Figure 6 shows the damping loss factors of the various subsystems, the coupling loss factors between the acoustic volumes and the panels, and the coupling loss factor between the acoustic volumes. Figure 7 shows the coupling loss factors between the fuselage and the three windshields. The fuselage was loaded by diffuse field excitation of a 258 $m^3$ exterior acoustic volume excited with a frequency independent input power of 1 W.

The dimensions of the fuselage plate, windshields, and interior volume were estimated based on an OpenVSP model of the reference aircraft (see Fig. 5). The fuselage was modeled as a 2 mm thick flat sheet of Aluminum ($E = 70$ GPa, $\nu = 0.33$, $G = 26$ GPa, $\rho_{Al} = 2700$ kg/$m^3$) with a surface area of 23 $m^2$. The area density of the fuselage was doubled to account for the frame, bulkheads,

***Figure 5:*** *CAD rendering of the NASA Lift+Cruise UAM representative aircraft.*

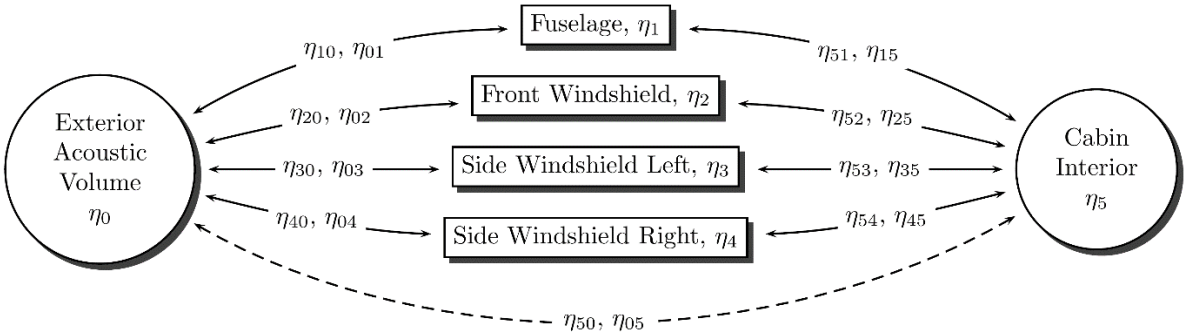


***Figure 6:*** *SEA subsystem damping loss factors and coupling loss factors between the acoustic volumes and the panels.*

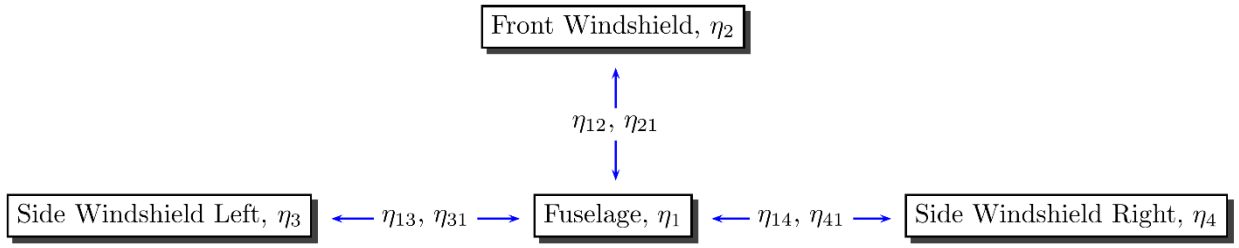


***Figure 7:*** *Plate to plate coupling loss factors between the fuselage and the three windshields.*

stringers or longerons, interior trim, and general system mass. Baseline or untreated windshields were modeled as 11.25 mm thick sheets of PMMA (E = 2.45 GPa, ν = 0.375, G = 1.7 GPa, $\rho_{pmma}$ = 1185 kg/m$^3$), which has an effective area density of 13.3 kg/m$^2$. The treated windshields were modeled as 15 mm thick sheets of PMMA with an equivalent area density of 13.3 kg/m$^2$ to account for the resonator cavities. The front windshield and side windshields were designated surface areas of 4 m$^2$ and 1.6 m$^2$, respectively, based on the OpenVSP model. The type 1 resonator had a surface area of $4.15\times10^{-3}$ m$^2$ and the treated front windshield contained 866 resonators while the side windshields each contained 346 resonators. The type 2 resonator had a larger surface area of $9.35\times10^{-3}$ m$^2$, therefore the front windshield contained 384 resonators while the side windshields each contained 153 resonators. The interior acoustic volume, which represents the cabin, was modeled as air with a volume of 12 m$^3$.

The SEA power balance equations of this structural-acoustic system require the coupling loss factors describing the mass law transmission from the exterior to the interior acoustic volume.[12–14] To calculate the mass law transmission coefficient without embedded resonators, a transmission coefficient for each panel was calculated. The diffuse field transmission coefficient for each panel can be calculated as[15]

$$\tau_d = \frac{\int_0^{\pi/2} \tau(\phi) \sin\phi \cos\phi d\phi}{\int_0^{\pi/2} \sin\phi \cos\phi d\phi}, \tag{9}$$

in which $\phi$ is the angle of incidence of an incoming sound wave. The plane wave transmission coefficient, $\tau(\phi)$, is calculated as

$$\tau(\phi) = \left| \frac{2z_{rad}}{2z_{rad} + z_p} \right|^2, \tag{10}$$

in which $z_{rad} = \rho_0 c_0 / \cos\phi$ is the assumed specific radiation impedance at the surface of the fuselage or windshields and the panel impedance of the fuselage or windshields is approximated as $z_p = j\omega m_s$, in which $m_s$ denotes the area density of the plate.

With embedded resonators, the plane wave transmission coefficient can be calculated as[16]

$$\tau(\phi) = \left| \frac{2z_t}{2z_{rad} + z_p} \right|^2, \tag{11}$$

in which $z_t$ is the total specific impedance of the radiating surface consisting of the partition and the resonator inlet openings. The specific radiation and resonator impedances are assumed to be a parallel acoustic circuit, and can be summed as such to calculate the total specific impedance as

$$z_t = \frac{1}{\frac{1-\sigma}{z_{rad}} + \frac{\sigma}{z_{in}}}, \tag{12}$$

in which $z_{in}$ is the specific input impedance of the resonator from Eq. (7) and the ratio of the resonator inlet areas to the panel surface area is given by

$$\sigma = \frac{N_r A}{S}, \tag{13}$$

in which $S$ is the panel surface area.

The individual transmission coefficients of each panel (fuselage and windshields) are multiplied by their percentage of the total surface area and summed together, resulting in the mass law transmission coefficient from the exterior acoustic volume to the cabin interior. Using the weighted transmission coefficients, it is straightforward to calculate the coupling loss factors between the exterior and cabin interior.[17]

The cabin interior reverberation time was assumed to be 0.5 sec, which was used to calculate the cabin's absorption area and damping loss factor. The damping loss factors of the fuselage and windshields are assumed to be 1% and the coupling loss factors between the acoustic volumes (exterior and interior) and each panel are calculated using the radiation resistance between each volume and panel.[18,19] A 1 W power input was applied to an exterior acoustic volume and the mean square sound pressure within the cabin interior was determined using the aforementioned model. The additional noise reduction (NR) due to the embedded resonators is calculated as

$$NR = 10\log_{10}\left( \frac{\overline{\langle p^2 \rangle}}{\overline{\langle p^2 \rangle}_{res}} \right), \tag{14}$$

in which $\overline{\langle p^2 \rangle}$ is the nominal mean square interior pressure and $\overline{\langle p^2 \rangle}_{res}$ is the mean square interior pressure with embedded resonators, both of which are band limited within 1/3 octave bands for the additional NR calculation.

### 3.2 Results

Results of various scenarios to evaluate the resonator concepts will now be presented and discussed. The following analyses will be limited to 1/3 octave bands below 1250 Hz because the half flexural wavelength of the PMMA material approaches the effective diameter of the type 1 resonator at around this frequency. Thus, the windshield model, which assumes a homogeneous plate, is not representative above this frequency. Note that of the subsystems included in the SEA model, the side windshields contain the fewest number of modes, ~9 in the 250 Hz 1/3 octave band, while the interior acoustic volume contains ~14 modes in this band.

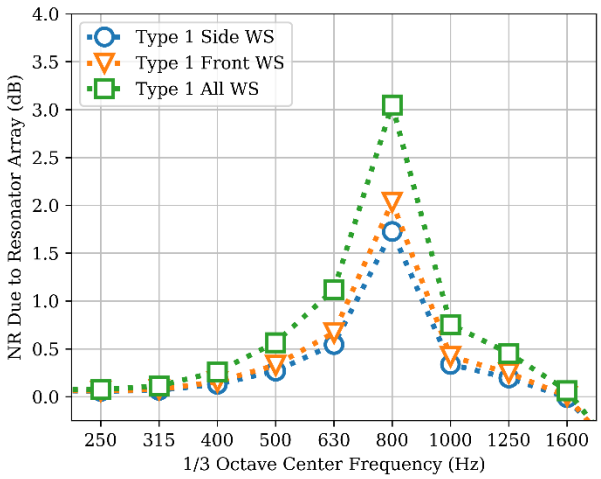


***Figure 8:*** *Noise reduction due to inclusion of type 1 resonators.*

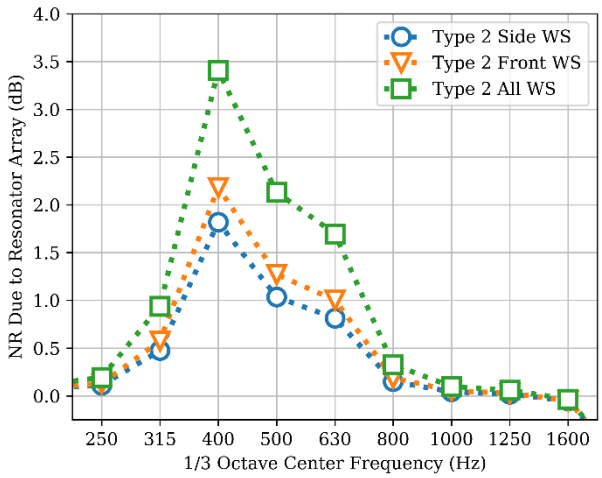


***Figure 9:*** *Noise reduction due to inclusion of type 2 resonators.*

Shown in Fig. 8 is the additional NR due to embedded type 1 resonators in the side windshields (blue), the front windshield (orange), and all windshields (green). Treating all windshields with type 1 resonators results in a maximum additional NR of 2.9 dB in the 800 Hz 1/3 octave band. Treating a larger surface area (i.e. treating all windshields) results in the highest reduction in noise.

Figure 9 presents the additional NR due to the inclusion of type 2 resonators in the side windshields (blue), the front windshield (orange), and all windshields (green). The maximum additional NR for type 2 resonators is 3.4 dB in the 400 Hz 1/3 octave band. The cavity size of the type 2 resonator is larger than that of the type 1 resonator, and thus targets a lower frequency, as mentioned previously. Once again, it is evident that treating a larger surface area results in a larger additional NR. In this case, fewer type 2 resonators are used due to the larger surface area. Regardless, the maximum additional NR is higher than the scenarios presented in Fig. 8.

Figure 10 shows the additional NR of four scenarios with a mixture of type 1 and type 2 resonators embedded in the front and side facing windshields. In blue, the front windshield was treated with type 2 resonators and the side windshields were treated with type 1 resonators. Conversely, in orange, the front windshield was treated with type 1 resonators, while the side

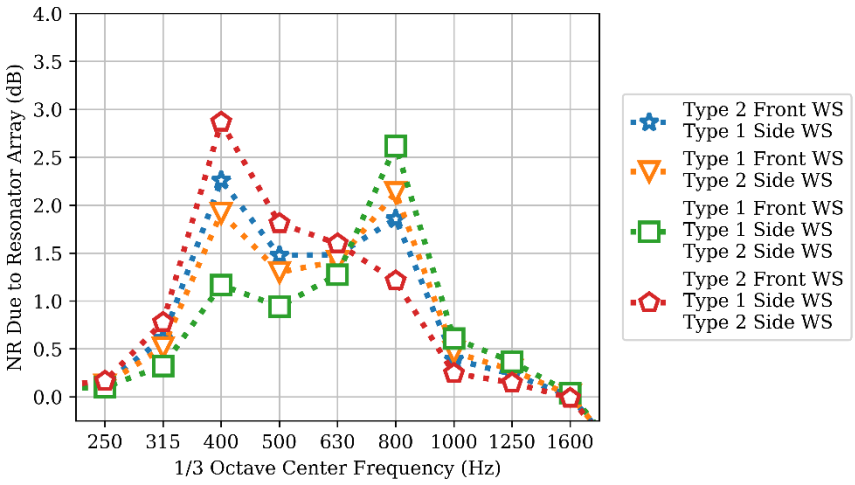


***Figure 10:*** *Noise reduction due to installation of a mixture of type 1 and type 2 resonators.*

windshields were treated with type 2 resonators. In green, the front windshield was embedded with type 1 resonators, while the side windshields were embedded with a mixture of type 1 and type 2 resonators. Due to the large surface area embedded with type 1 resonators, this configuration resulted in the highest additional NR of 2.6 dB in the 800 Hz 1/3 octave band, but resulted in the lowest additional NR in the lower octave bands. In red, the front windshield was treated with type 2 resonators with type 1 resonators embedded in one of the side windshields and type 2 resonators in the other. This configuration resulted in a maximum additional NR of 2.9 dB in the 400 Hz 1/3 octave band as well as the highest additional NR in the 500 and 630 Hz 1/3 octave bands, and the lowest additional NR in the 800 Hz 1/3 octave band.

## 4 CONCLUSION

This paper presented a preliminary investigation into the additional noise reduction that embedded windshield resonators could provide in the cabin of a UAM concept vehicle. Two hexagonal concepts were evaluated; one had an internal hex radius of 40 mm while the other had an internal hex radius of 60 mm.

SEA was used to calculate the additional noise reduction of the embedded resonators compared to the noise reduction of the untreated windshield. The model considered was an aircraft fuselage with a cabin volume of 12 $m^3$ and an exterior surface area of 30.2 $m^2$, 24% of which consisted of windshields. The fuselage subsystems in the SEA model were assumed to be flat plates. The exterior acoustic volume was excited with a diffuse field with an input power of 1 W for the purposes of generating an interior acoustic response. The model was assumed to be appropriate for a frequency range of 400 to 1000 Hz 1/3 octave bands. The SEA calculations confirmed that the larger resonator targeted lower frequencies (~400 to ~700 Hz) while the smaller resonator targeted higher frequencies (~830 Hz). Inclusion of larger resonators in the front and side windshields resulted in a maximum additional noise reduction of 3.4 dB in the 400 Hz 1/3 octave band while inclusion of smaller resonators resulted in a maximum additional noise reduction of 2.9 dB in the 800 Hz 1/3 octave band. Note that fewer of the large resonators could be incorporated into a windshield than the smaller resonators due to the larger surface area coverage; despite this, the results showed a larger maximum additional noise reduction when using the larger resonators. Using a mixture of the two resonator types could provide additional noise reduction across a broader range of frequencies, albeit at a lower level than using only one type of resonators. As a result, it may be desired to design a resonator to target the operating BPF of an aircraft.

There are benefits to this concept that warrant further research. For one, the concept does not require structural modification to the aircraft aside from the windshield. Additionally, a windshield embedded with resonator cavities could be designed to have an equivalent weight to a nominal windshield – which provides an additional noise treatment without an increase in mass. This is a primary benefit over most noise treatment options. A limitation of this design is obviously potentially reduced vision. Further investigation is necessary to design a package that conforms to requirements related to crash worthiness, cost, bird strikes, and of course, visibility.

Future work could focus on different combinations of resonator geometries. Additionally, samples could be built for transmission loss testing in the NASA Langley's Structural Acoustics Loads and Transmission (SALT) facility. As the introduction of resonator cavities within the multilayer windshields will introduce optical scattering effects, their impact on visibility requirements would also need to be considered.

## ACKNOWLEDGEMENTS

M. Galles thanks Mr. Eduardo Solis of the Science & Technology Corporation for images of the NASA Lift+Cruise reference aircraft. The Revolutionary Vertical Lift Technologies Project supported this work under the Advanced Air Vehicles program at the National Aeronautics and Space Administration.

## REFERENCES

1. C. Silva, W. R. Johnson, M. D. Patterson, and K. R. Antcliff, "VTOL Urban Air Mobility Concept Vehicles for Technology Development". *Proc. 2018 Aviation Technology, Integration, and Operations Conf*. Atlanta, Georgia, (2018).
2. S. Polychronopoulos, D. Kougias, P. Polykarpou, and D. Skarlatos, "The Use of Resonators in Ancient Greek Theatres", *Acta Acust. united Ac.* **99(1)**, 64–69 (2013).
3. R. G. Arns, and B. E. Crawford, "Resonant Cavities in the History of Architectural Acoustics", *Technology and Culture* **36(1)**, 104–135 (1995).
4. H. L. Kuntz, R. A. Prydz, F. J. Balena, and R. J. Gatineau, "Development and Testing of Cabin Sidewall Acoustic Resonators for the Reduction of Cabin Tone Levels in Propfan-Powered Aircraft", *Noise Control Eng. J.* **37(3)**, 129 (1991).
5. S. A. Lane, R. E. Richard, and S. J. Kennedy, "Fairing Noise Control Using Tube-Shaped Resonators", *J. Spacecr. Rockets* **42(4)**, 640–646 (2005).
6. A. Allen, N. Schiller, and J. Rouse, "Noise Control Capability of Structurally Integrated Resonator Arrays in a Foam-Treated Cylinder", *SAE Int. J. Veh. Dyn., Stab., and NVH* **1(2)**, 362–371 (2017).
7. K. U. Ingard, *Noise Reduction Analysis*, Jones and Bartlett Publishers, Boston, 2010.
8. A. D. Pierce, *Acoustics: Introduction to its Physical Principles and Applications*, Acoustical Society of America, Woodbury, New York, 1989.
9. W. M. Leach, Jr., *Introduction to Electroacoustics and Audio Amplifier Design*, Kendall-Hunt, Dubuque, Iowa, 2003.
10. Dassault Systèmes Simulia Corp, *Abaqus/CAE 2018*, Johnston, Rhode Island, 2018.
11. F. Jacobsen, and P. M. Juhl, *Fundamentals of General Linear Acoustics*, Wiley, Chichester, 2013.
12. R. H. Lyon, and R. G. DeJong, *Theory and Application of Statistical Energy Analysis*, Elsevier Science, Boston, 1995.
13. R. J. M. Craik, *Sound Transmission through Buildings using Statistical Energy Analysis*, Gower, United Kingdom, 1996.
14. S. A. Hambric, S. H. Sung, and D. J. Nefske, *Engineering Vibroacoustic Analysis: Methods and Applications*, Wiley, West Sussex, United Kingdom, 2016.
15. F. Fahy, and P. Gardonio, *Sound and Structural Vibration: Radiation, Transmission and Response*, Elsevier/Academic, Boston, 2007.
16. N. H. Schiller, A. R. Allen, B. F. Zalewski, and B. S. Beck, "Sound Transmission Loss Through a Corrugated-Core Sandwich Panel With Integrated Acoustic Resonators". *Proc. ASME 2014 International Mechanical Engineering Congress and Exposition*. Montreal, Quebec, Canada, (2014).
17. M. P. Norton, and D. G. Karczub, *Fundamentals of Noise and Vibration Analysis for Engineers*, Cambridge University Press, Cambridge, 2003.
18. G. Maidanik, "Response of Ribbed Panels to Reverberant Acoustic Fields", *J. Acoust. Soc. Am.* **34(6)**, 809–826 (1962).
19. G. M. L. Gladwell, and J. Wijker, *Random Vibrations in Spacecraft Structures Design: Theory and Applications*, Springer Netherlands, Dordrecht, 2009.